MATERIALS PHYSICS AND MECHANICS RESEARCH ARTICLE

Submitted: June 21, 2025 **Revised: September 8, 2025** **Accepted: November 4, 2025**

Strength characteristics of additively manufactured meta-biomaterials made of titanium alloy under cyclic loading

L.B. Maslov [1,2], A.I. Borovkov [1], L.S. Nezhinskaya [1], M.A. Zhmaylo [1]✉, F.D. Tarasenko [1]

[1] Peter the Great St. Petersburg Polytechnic University, St. Petersburg, Russia

[2] Ivanovo State Power Engineering University n.a. V.I. Lenin, Ivanovo, Russia

✉ zhmaylo@compmechlab.com

ABSTRACT

The study considers the fatigue strength of additively manufactured specimens made of metamaterials based on Ti-6Al-4V titanium alloy. The study presents results of full-scale tests for two types of meta-biomaterials: lattice and surface. Dynamic tests were performed in a symmetrical tension-compression cycle at room temperature. The goal of the tests was to construct an S-N curve, which was used to determine the fatigue limit of the metamaterial. We found that the results of numerical simulation differ significantly from the full-scale tests, showing a trend toward overestimated fatigue life. The surface roughness parameter of the specimen was introduced, allowing to achieve better agreement between the results of full-scale tests and numerical simulations.

KEYWORDS

metamaterial • titanium alloy • lattice structures • surface structures • fatigue strength • finite element analysis

Funding. *The research was funded by the Russian Science Foundation (project No. 23-19-00882), https://rscf.ru/project/23-19-00882.*

Citation: Maslov LB, Borovkov AI, Nezhinskaya LS, Zhmaylo MA, Tarasenko FD. Strength characteristics of additively manufactured meta-biomaterials made of titanium alloy under cyclic loading. *Materials Physics and Mechanics*. 2025;53(5): 50–73.
http://dx.doi.org/10.18149/MPM.5352025_4

Introduction

Structures created in various branches of modern high-tech engineering (aerospace, automotive, aircraft, shipbuilding, etc.) require materials combining high strength with resistance to cyclic loads. Titanium alloys, in particular Ti-6Al-4V (or its Russian equivalent VT6), have remained a key structural material for several decades due to the optimal ratio of strength, corrosion resistance and durability under dynamic loads [1]. Metamaterials based on the Ti-6Al-4V alloy have also been the focus of considerable attention in modern biomedical technologies, in particular, in traumatology, orthopaedics and regenerative medicine, due to biocompatibility, lightness and strength of titanium.

Metamaterials with an artificially produced periodic structure exhibit unique mechanical characteristics, including negative Poisson's ratios, controlled anisotropy and good fatigue strength compared with traditional solid materials with isotropic properties. The designed elastic and strength properties of lattice and surface metamaterials based on Ti-6Al-4V titanium alloy expand their scope of application in the aerospace industry,

© L.B. Maslov, A.I. Borovkov, L.S. Nezhinskaya, M.A. Zhmaylo, F.D. Tarasenko, 2025.
Publisher: Peter the Great St. Petersburg Polytechnic University
This is an open access article under the CC BY-NC 4.0 license (https://creativecommons.org/li-censes/by-nc/4.0/)

biomedicine and other fields with demand for materials with unique mechanical properties [2].

As additive technologies are gaining increasing popularity [3], new approaches must be developed to evaluating the strength characteristics of metal-based metamaterials. The physical behaviour of Ti-6Al-4V alloy serving as a base material for 3D printing of metamaterials has been comprehensively explored to study various additive technologies for manufacturing tests specimens, such as electron beam melting (EBM), selective laser melting (SLM), laser powder bed fusion (LPBF) [4]. It was found that the mechanical properties of additively manufactured titanium alloy after appropriate thermal treatment were within the standard range of parameter values for solid materials fabricated by conventional methods [5,6].

Material fatigue is understood as the gradual accumulation of damage in the material under the influence of variable stresses, typically below the yield point, leading to cracking and fracture [7]. The fatigue strength of materials under variable cyclic loading largely depends on the time evolution of stresses; the loads considered are typically periodic. It was experimentally established that the number of cycles to failure depends not only on the magnitude of the maximum absolute stress but also on the stress amplitude of the cycle. The larger this quantity at constant maximum stress, the fewer loading cycles the material can withstand. For many materials, there is a maximum cycle stress at which the material can withstand an infinite number of load cycles. The highest absolute stress in the cycle at which fatigue failure does not yet occur is called the fatigue limit of the material. The fatigue limit of the material is determined by testing identical specimens at different values of maximum stress with a constant asymmetry coefficient, recording the number of cycles at which failure occurs in each specimen. The number of cycles that the specimen or part can withstand before failure characterizes the fatigue life of the material.

High-cycle fatigue occurs at stresses well below the yield point. In this case, the material is elastically deformed, so its properties are satisfactorily described by Hooke's law. Since most materials have a complex multicomponent structure (grains, pores, non-metallic inclusions, etc.), alternating local plastic deformation, which is called microplastic, occurs in individual microvolumes under elastic deformation of a sufficiently large volume. As this deformation is repeated for multiple cycles, microscopic cracks start to evolve. The boundary between low-cycle and high-cycle fatigue is not clearly defined. The fatigue life of 10^5 cycles can be selected as the threshold for Ti-6Al-4V alloy [8].

Traditional experimental methods for evaluating the fatigue characteristics of metals include symmetric cyclic loading controlling the number of cycles to failure, which allows to construct Wöhler fatigue curves, or the so-called S-N (stress-number) curves [9]. The maximum cycle stress at which the specimen is tested is plotted along the ordinate, and the number of cycles that the specimen can withstand until failure is plotted along the abscissa. According to standard approaches to fatigue strength testing, at least fifteen identical specimens are tested to build a fatigue curve and determine the fatigue limit.

Studies show that fatigue life strongly depends on the microstructure: coarse-grained structures show higher resistance to crack initiation, while fine-grained structures show higher resistance to crack propagation [10]. The fatigue characteristics of Ti-6Al-4V fabricated by the traditional technique and laser power bed fusion (LPBF) are compared in [11].

It was found that additively manufactured specimens have 15–20 % lower fatigue life due to the presence of pores and residual stresses. This confirms the need for post-treatment (thermal or mechanical) to improve performance.

A distinctive characteristic of metamaterials is that their properties are architecture-dependent. Lattice structures can exhibit greater fatigue strength compared to classical solid materials with the same density. However, the location of the crack initiation site becomes critical, as failure generally begins in the connections between strut elements. Failure in even a small number of struts in a lattice structure greatly reduces the load-bearing capacity of the structure [12].

Additive manufacturing of products from metamaterials often faces problems with fatigue strength, primarily due to manufacturing quality. Despite high accuracy of modern 3D printers, internal defects occur in the material at the micro, meso, and macro levels during the printing process [13]. Such defects often have a significant influence on the mechanical characteristics and behaviour of the metamaterial during its service life [14]. Depending on the geometric location and shape, these defects negatively affect the strength and other mechanical properties of the complex structure of the metamaterial as a whole [15].

The complex architecture of metamaterials makes classical experimental testing methods too cumbersome, which stimulates the development of computational approaches to evaluating the strength properties of complex elastic structures. Numerical technologies actively pursued to study mechanical fatigue include mathematical modelling methods such as finite element analysis (FEA), discrete element method (DEM) for modelling fracture in brittle structures and multilevel modelling at micro, meso, and macroscales. The crystal plasticity finite element method (CPFEM) accounting for plasticity and crack kinetics for metal alloys allows to build models characterizing grain orientation and dislocation dynamics to predict fatigue life with a small error in comparison with full-scale tests [16].

Despite the progress made in this area, several major issues remain unresolved. Crucial aspects of fatigue testing include the scale effect on test results (real designs exhibit significant differences from laboratory specimens in cyclic loading); the influence of defects, for example, randomly distributed pores in the volume of additively manufactured material; the effect of dynamic loading rate, which is critical for components of turbines, rockets, and airplanes.

A promising direction is integration of machine learning, for example, neural network predictions of fatigue life based on microstructural data. For example, the machine learning method was used in [17] to study the influence of location, size and morphology of defects inside the structure to improve the prediction of fatigue life.

The full-scale tests and simulations carried out in this paper to obtain the strength characteristics of additively manufactured metamaterials under cyclic loading used the following unit cells of a meta-biomaterial based on Ti-6Al-4V alloy: gyroid, a surface-based meta-biomaterial, and diamond, a lattice-based meta-biomaterial. All metamaterials have three porosity values of 30, 50, and 70 %. High-cycle tests are performed to evaluate the parameters characterizing fatigue in the metamaterial under the influence of long-term loads with amplitudes below the yield strength.

Materials and Methods

The base material was a Ti-6Al-4V alloy in the form of spherical powder with particle sizes from 15 to 53 μm with a chemical composition of 90.02 wt. % Ti, 6.01 wt. % Al, 3.89 wt. % V, 0.08 wt. % Fe. The alloy is widely used in surgical operations to replace bone structures with artificial components due to its high strength properties, chemical stability and biocompatibility. It can be used to manufacture parts with thin elements and complex geometries, also well suited to manufacturing products whose mass should be minimal.

Geometric models

To evaluate the fatigue characteristics of metamaterials with complex internal structure, it is important to understand the behaviour of the solid material from which the metamaterial is fabricated. The mechanical behaviour and representative values of elastic and strength properties of the biocompatible Ti-6Al-4V alloy are well known, available in Russian [6] and foreign [5,10] reference books and databases of materials. In this study, we carried out an experimental evaluation of the mechanical properties of solid material additively manufactured with a 3D printer to assess the reliability of the test results for metamaterials obtained by similar technologies.

We considered solid specimens for cyclic loading tests, whose shape and dimensions are standardized in GOST 25.502-79 [18]. The specimen models were built in the SolidWorks CAD software. The appearance and geometric characteristics (total length of 108 mm, thickness of 3 mm, length and radius of the gauge section of 28 and 25 mm, respectively) of the model are shown in Fig. 1.

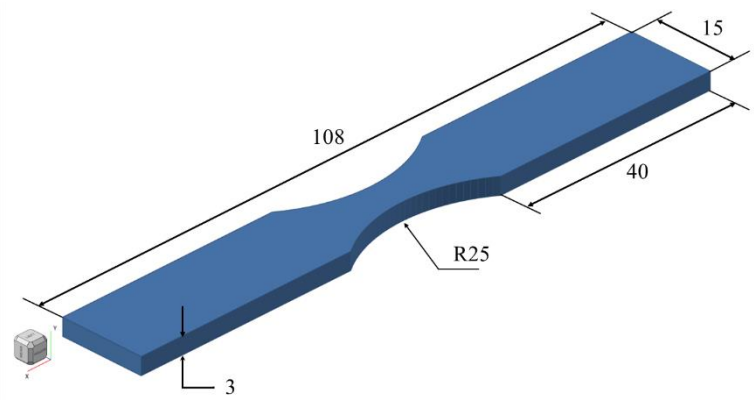

Fig. 1. Solid specimen for fatigue tests

The following types known from the literature were selected as representative volume elements (RVE's), or unit cells, of the fabricated metamaterials: diamond, a cell composed of short struts making up a diamond crystal lattice; gyroid, a cell based on triply periodic minimal surfaces (TPMS).

The volume fractions of solid material were taken to be 30, 50 and 70 %. The variation in porosity of RVE's and, accordingly, specimens of the metamaterial is regulated by the diameter of the struts making up the diamond lattice metamaterial or by the thickness of the 'trabeculae' formed by periodically repeating surfaces shifted by a fixed

distance relative to each other in the case of the metamaterial based on TPMS. In the latter case, the introduced thickness is the characteristic transverse dimension of curved solid shell elements forming surface-based metamaterials.

The following factors were taken into account to design CAD models of the specimens for printing:

1. at least five unit cells had to be included along all axes of the gauge section of the specimen to minimize the influence of local factors on the overall deformation behaviour;
2. minimum thickness of the RVE was limited to 1 mm for additive manufacturing to reduce the impact of manufacturing defects on experimental results;
3. grip section for specimens subjected to tensile loading was substantially long, at least 42 mm;
4. specimen stiffness in the grip section was at least 1.5 times as high as that in the gauge section;
5. material for the specimens had to be used judiciously to reduce the manufacturing costs.

Geometric models of metamaterial cells were built in the Altair Inspire 2023 software, allowing to create models of periodic porous structures of various topologies (Fig. 2). Unit cells of lattice and surface metamaterials and the construction of their models are described in our earlier studies [19,20].

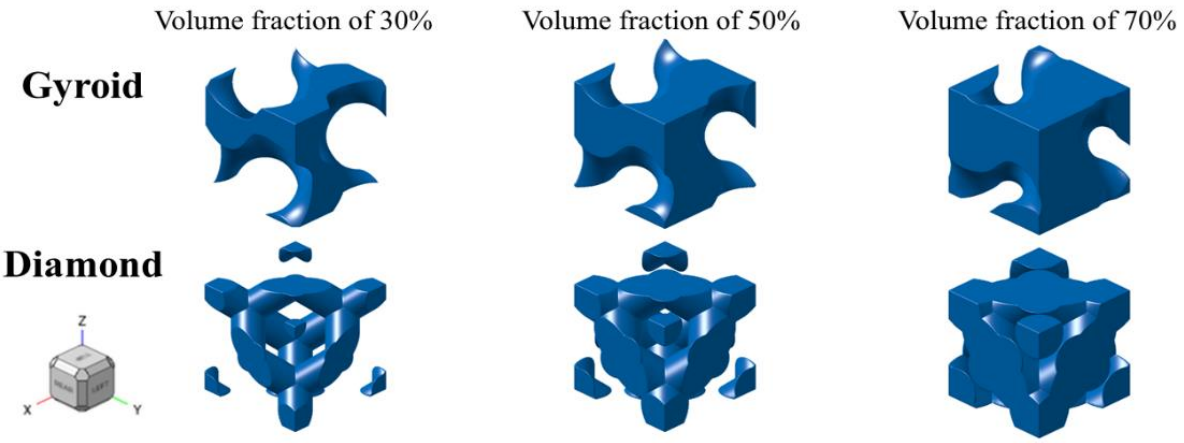

Fig. 2. CAD models of unit cells for constructing gyroid and diamond metamaterials with three volume fractions of solid material: 30, 50 and 70 %

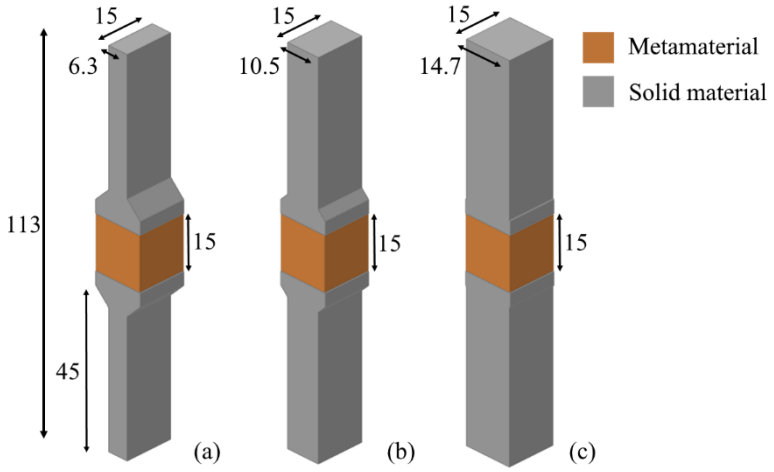

Fig. 3. Characteristic shape and dimensions of specimens for cyclic loading tests: (a) specimen with 30 % volume fraction of solid material, (b) specimen with 50 % volume fraction of solid material, (c) specimen with 70 % volume fraction of solid material

The two basic 3D structures (diamond, gyroid) with three characteristic porosities (30, 50 and 70 %) were used to build 3D CAD models, necessary for 3D printing of specimens for subsequent mechanical testing. The characteristic (including overall) dimensions and shape of the specimens for cyclic loading are shown in Fig. 3.

The given volume of the metamaterial (Fig. 4) with the dimensions of 15 × 15 × 15 mm^3 and a unit cell size of 3 × 3 × 3 mm^3 was designed in Altair Inspire 2023 and complemented by massive solid grips with a length of 45 mm, with the cross-sectional area of the grip exceeding the effective area of the specimen's gauge section by at least 1.5 times (Fig. 5). Such a restriction ensures that failure occurs within the gauge section of the specimen, allowing to correctly evaluate the deformation in the metamaterial, eliminating the influence of solid grips.

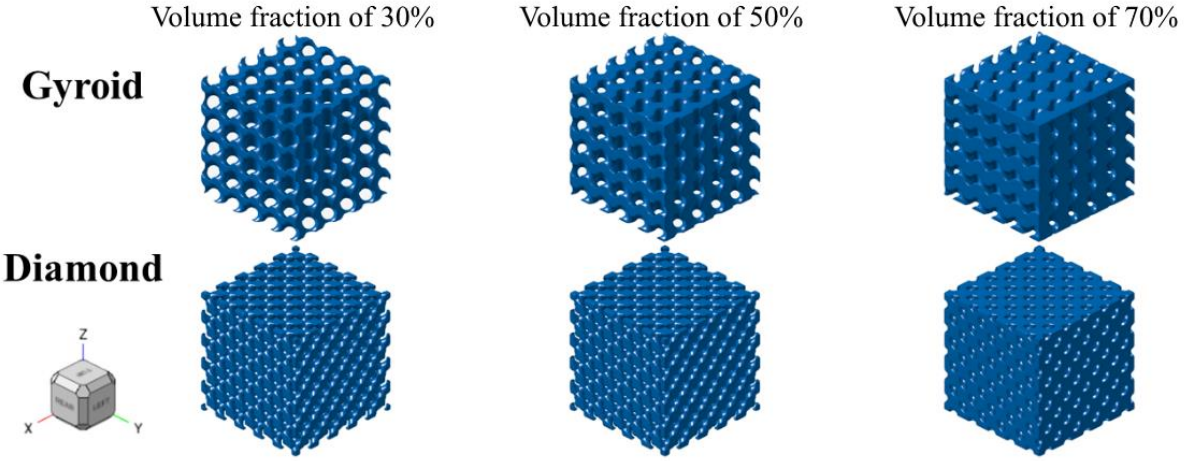

Fig. 4. CAD models of metamaterial specimens (gyroid, diamond) with three volume fractions of solid material (30, 50 and 70 %)

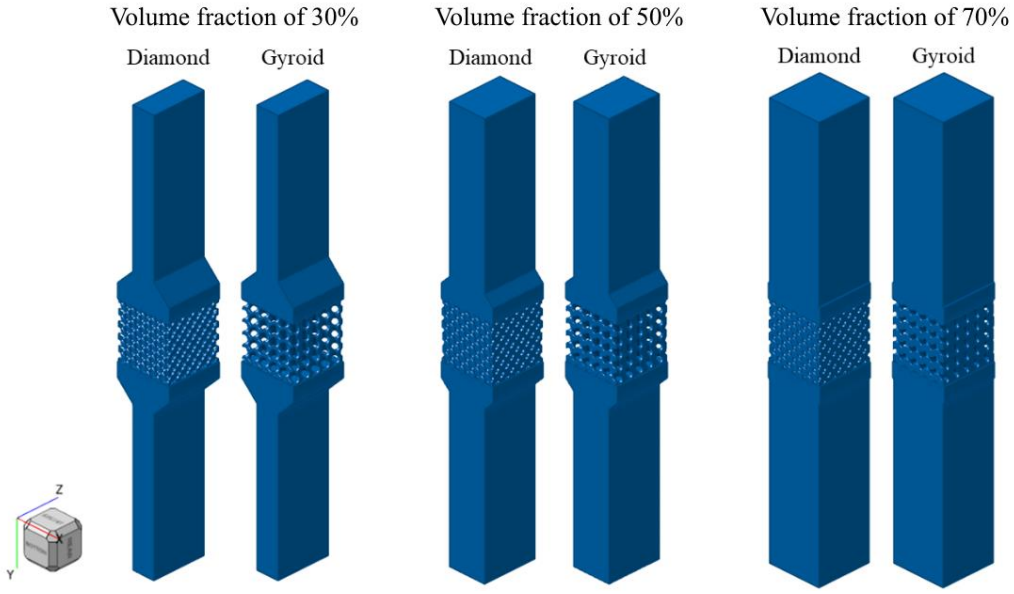

Fig. 5. CAD models of metamaterial specimens (diamond and gyroid) with three volume fractions of solid material (30, 50 and 70%) for full-scale tests on cyclic loading

The lattice-based diamond structure was designed with the strut thickness set equal to 0.4, 0.56, 0.71 mm for volume fractions of 30, 50 and 70 %, respectively. The surface-based gyroid structure is designed with the required volume fraction set from 0 to 1, where 0 is the absence of material and 1 is solid material. In our case, the volume fractions were 0.3, 0.5 and 0.7. The obtained minimum thicknesses of the "trabeculae" for the gyroid structure were 0.97, 35 and 1.87 mm.

Specimens for full-scale tests

Solid specimens (15 pieces) from additive titanium alloy for testing were additively manufactured by selective laser melting on a Concept Laser M2 industrial 3D printer (GE Additive, Germany) with the printing area of 250 × 250× 280 mm^3 (Fig. 6). A biocompatible Ti-6Al-4V powder was used for 3D printing of specimens from additive material.

(a) (b)

Fig. 6. 3D-printing equipment and prepared Ti-6Al-4V specimens: (a) Concept Laser M2 industrial 3D printer, (b) 3D-printed solid specimens for testing

The metamaterial specimens based on the designed geometric models were prepared by SLM from biocompatible Ti-6Al-4V powder also using the Concept Laser M2 printer. A series of specimens with three volume fractions was prepared for each of the two types of metamaterials for cyclic loading tests. Examples of additively produced specimens are shown in Fig. 7. A total of 12 specimens (2 identical specimens of each type) were printed for full-scale tests of metamaterials.

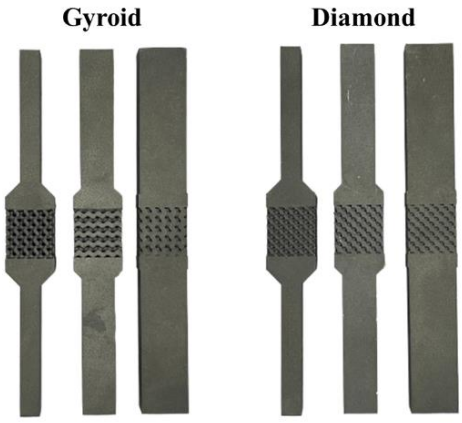

Fig. 7. Front view of printed metamaterial specimens based on Ti-6Al-4V alloy (gyroid and diamond) with three volume fractions of solid material (30, 50 and 70 %) for full-scale tests on cyclic loading

Evaluation of material density

Because the metamaterial specimens for full-scale testing are manufactured additively and have a complex structure, their volume and geometric characteristics differ from the nominal characteristics of the corresponding CAD models. The specimens for full-scale tests are dry-weighed, with the actual porosity of the meta-biomaterial subsequently determined, which allows to adjust the geometry of the specimen model to reproduce the experiments in a simulation environment and bring the model parameters closer to the characteristics of the printed specimen.

To calculate the actual volume fraction, or volume content, of solid material in a metamaterial, in addition to the mass of the samples, the density of the titanium alloy used in printing the samples is determined. By weighing fifteen solid samples of the same type made for fatigue testing and calculating the average mass of one sample and based on the sample volume known from its digital model, simple calculations can be used to obtain the density of the solid material based on the additive titanium alloy. Then, to calculate the value of the actual volume fraction of the solid phase of the metamaterial of each sample, it is necessary to consider the lattice structure of the metamaterial without taking into account the grips added to the metamaterial sample for its attachment in the testing machine.

$$\varphi = \frac{\rho_{lattice}}{\rho_{Ti6Al4Vi}}, \quad (1)$$

$$\rho_{lattice} = \frac{m_{lattice}}{V_{lattice}}, \quad (2)$$

$$m_{lattice} = m_{sample} - m_{grips}, \quad (3)$$

$$m_{grips} = V_{grips} \cdot \rho_{Ti-6Al-4V}, \quad (4)$$

where φ is the volume fraction of the solid phase of the metamaterial; $\rho_{lattice}$ is the effective density of the metamaterial, defined as the ratio of the mass of the metamaterial specimen under consideration to its overall volume; $\rho_{Ti-6Al-4V}$ is the actual density of the Ti-6Al-4V titanium alloy used; $m_{lattice}$ is the mass of the metamaterial specimen under consideration, in this study in the form of the cube of 15 × 15 × 15 mm^3; $V_{lattice}$ is the overall volume of the metamaterial specimen under consideration, equal to 3.375 mm^3; respectively, m_{sample} is the mass of the entire printed test specimen consisting of the cube of metamaterial and additional grips; m_{grips} is the mass of additional solid titanium alloy grips for attaching the specimen in the machine added to the metamaterial specimen; V_{grips} is the volume of the additional grips.

After the relative density of the periodic structure of the specimens is determined, the numerical model is corrected to take into account the obtained volume fractions and is used for reproducing full-scale tests in the simulation environment. In the case of lattice specimens, the thickness of the strut is varied in accordance with the obtained relative density of the meta-biomaterial; in the case of the surface structure, the geometry is adjusted directly by setting the actual volume fraction.

Testing procedure for determining fatigue properties

The purpose of the cyclic tests was to construct the S-N curve to subsequently determine the fatigue limit of the solid material. In our case, tests were carried out for 15 solid specimens up to their fracture under various loads. Cyclic loading tests to determine the

fatigue properties at room temperature were carried out on a Zwick Roell AMSLER 100 machine (Fig. 8) with testXpert V12.3 software. A resonant system with variable loading frequency was used in the experiments, allowing to adjust the loading frequency to ensure stable loading in the selected range.

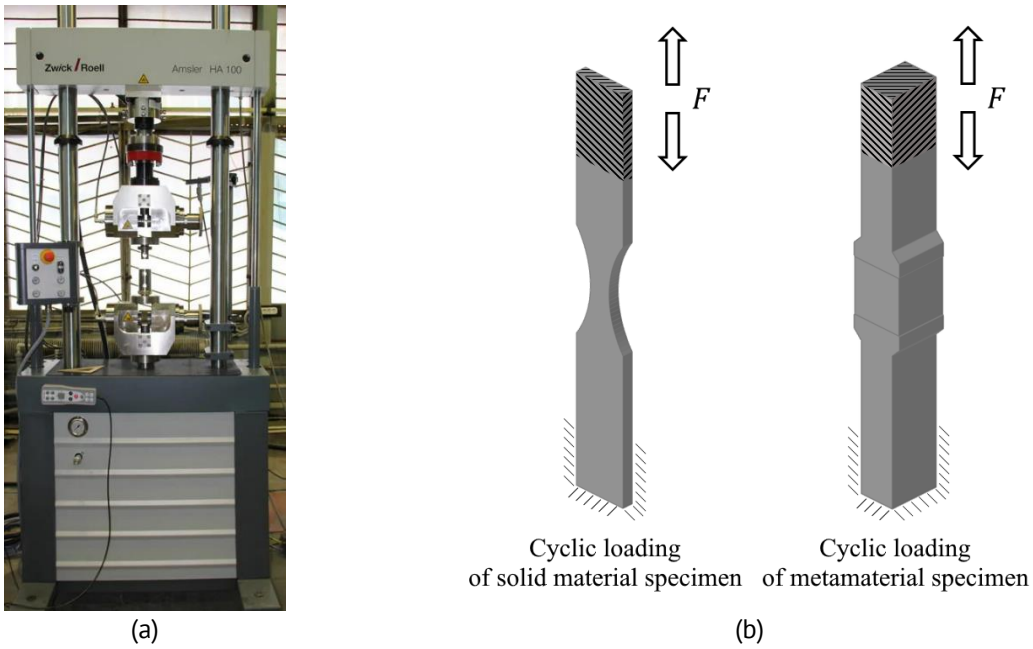

Fig. 8. Experimental equipment and loading conditions for cyclic loading tests: (a) Zwick Roell AMSLER 100 system, (b) loading conditions for solid specimens and metamaterial specimens

The uniaxial stress state of the test specimen is characterized by the load cycle asymmetry coefficient $R = \sigma_{max}/\sigma_{min}$, where σ_{min} and σ_{max} are the minimum and maximum values of stresses applied to the specimen in the load cycle. Tests for constructing the S-N curve and determining the fatigue characteristics of the solid material are usually carried out with a symmetrical tension-compression cycle, when $\sigma_{min} = -\sigma_{max}$. For each tested specimen, the loading amplitude, the number of fracture cycles, and the cyclogram were recorded. Testing of one speciment before reaching the destruction forms one point of the S-N curve in the coordinates "force – number of loading cycles".

According to GOST 25.502-79 [18], at least 15 identical specimens are tested to build a fatigue curve and determine the fatigue limit corresponding to a 50 % probability of failure. At least three specimens are tested within the 0.95–1.05 fatigue limit stress range, corresponding to a 50 % probability of failure, and at least half of them must not fracture within the selected number of test cycles. In our case, the number of cycles for determining the fatigue limit is taken equal to 2 million.

The test results are used to plot points on the axes corresponding to the number of cycles versus stress amplitude in log-log coordinates. The fatigue curve is plotted in log-log coordinates based on the test results of the specimens after processing the experimental data using the least squares method. The left, inclined branch of the fatigue curve is described by the equation of the form:

$$\sigma_a(N) = A \cdot N^{-B}, \quad (5)$$

where $\sigma_a(N)$, MPa, is the stress amplitude of the cycle; A is the coefficient corresponding to the maximum stress that the material can withstand in one loading stage, approximately corresponding to the intersection of the curve with the ordinate axis; N is the fatigue life expressed as the number of cycles for a given stress amplitude; B is the exponent characterizing the slope of the straight line plotted in log-log coordinates using the least squares method from the points corresponding to the test results.

The right branch of the fatigue curve is a horizontal straight line. The coefficients of the obtained fatigue curve are calculated in the postprocessing software, provided together with the experimental data for each specimen. The experimental data is processed based on the technique described in [21].

One of the main factors influencing the results of high-cycle fatigue testing for metamaterials is the surface roughness in the gauge section. Additive manufacturing technologies using metal powders provide a relatively low quality of the surface, with local structural defects observed. A possible solution to this problem is mechanical processing of the obtained specimens. However, such processing was not included in the experimental plan, since the goal of this study was not to obtain the most durable specimens through additional manipulations, but rather to determine the mechanical characteristics of meta-biomaterials under conditions best reproducing their real-life cycle.

In view of this, the following factors were taken into account to determine the fatigue properties of metamaterials: more predictable, reproducible behaviour close to solid material for specimens with the high volume fraction, which is why such specimens were tested first; the yield strengths found in previous experiments for similar specimens [22], allowing to evaluate the upper bound for the load amplitude multiplied by 0.8; accounting for the S-N curve obtained for solid material and the fatigue limit.

After a series of preliminary experiments was conducted and the first results were obtained, we found that the most effective technique for predicting the stress amplitude turned out to be the comparing the yield strength ratios for the solid and the metamaterial with the fatigue limit ratios for the same specimens. The tests were repeated for 2 million cycles. After that, the specimen was considered unfractured. In some cases, the duration of the test was increased to assess whether the selected bound was correct.

Finite element models of metamaterials and specimens

Computational mathematical models based on the finite element method were developed based on the prepared 3D CAD models of the specimens made of solid material and two types of metamaterials. Full-scale tests on fatigue strength were reproduced in a simulation environment in two stages. The first stage was uniaxial tension for each metamaterial specimen in the Abaqus software, describing a half-cycle (symmetric tension-compression cycle) of the fatigue test. The procedures for developing the numerical models and performing the simulations were done in Abaqus. The problems were solved on a workstation equipped with Intel Xeon Silver 4210R processor (2.4 GHz, 12 cores).

Finite element meshes for the models of metamaterials considered are given in Fig. 9, schematically showing the kinematic boundary conditions of the solved problem on tension of a deformable solid by the displacements set along the specimen axis. Fixed

zero displacements of the mesh nodes at one end of the specimen simulate rigid fixation of the specimen in the grips of the testing machine, while the given non-zero component of the displacements along the specimen axis simulates the movements of the crosshead.

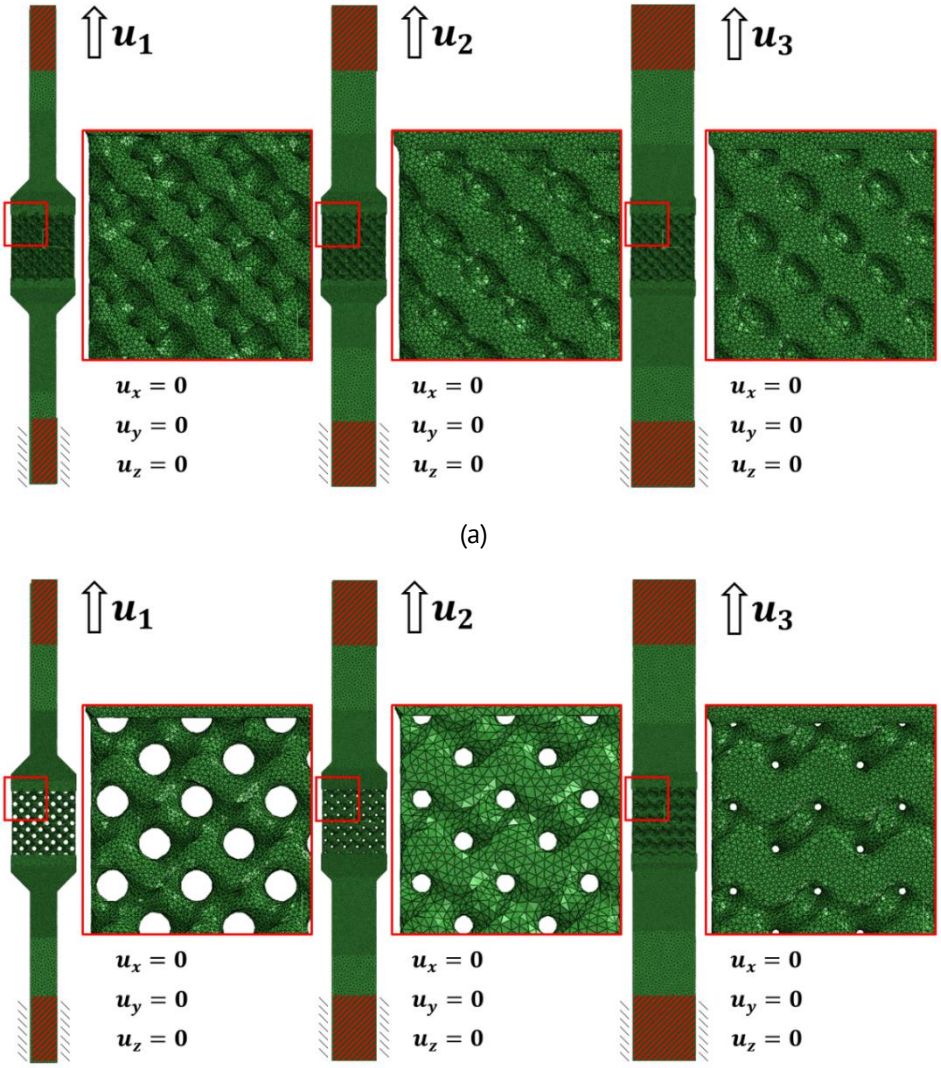

Fig. 9. Schematics for design of numerical tests on uniaxial tension of metamaterial specimens and fragments of finite element mesh: (a) diamond, (b) gyroid. The specimens with 30, 50 and 70 % volume contents of titanium alloy are shown from left to right

The load application region is kinematically coupled to the reference point, for which a non-zero displacement in the longitudinal direction is set. The displacement value is selected so that the final deformation of the specimen's gauge corresponds to the deformation obtained in the full-scale test. The displacement value during the tensile tests varies linearly from zero to a maximum equal to 3, 4, and 5 mm for specimens with the metamaterials of the considered volume fractions (Fig. 9).

In the case of numerical tests of the metamaterial, the size of the finite element in the gauge section of the metamaterial specimens was 0.1 mm due to geometric complexity of the internal structure. The quantitative characteristics of the finite element meshes are given in Table 1. The resulting files with the computational results are

imported from Abaqus into the Altair HyperLife environment for the second stage of simulation evaluating the fatigue properties of the model.

Table 1. Quantitative characteristics of finite element models of metamaterial specimens for numerical simulations

Specimen	Nodes	Elements
Diamond, 30%	304 396	1 210 275
Gyroid, 30%	249 756	988 563
Diamond, 50%	297 937	1 232 168
Gyroid, 50%	96 911	402 611
Diamond, 70%	299 051	1 266 728
Gyroid, 70%	261 777	1 104 826

Simulation procedure for high-cycle fatigue tests

Numerical simulations reproducing the fatigue tests were performed in the Altair HyperLife 2023.1 fatigue analysis software, using basic solvers, including support for post-processing of stress results from the Abaqus environment. Setting up fatigue tests in the computational environment requires importing a solver file with the results of finite element analysis of the specimen, specifying the parameters of the material model and specifying the fatigue curve for a symmetrical loading cycle. The files with the results of quasi-static simulations for uniaxial tension of diamond and gyroid specimens with the volume fractions of 30, 50 and 70 % of solid material were taken as input files for fatigue analysis.

Loading steps from Abaqus are recognised in Altair HyperLife, each step corresponding to a specific force, which is a response to the displacement applied to the specimen during the simulation of uniaxial tension. The loading step for the numerical test is selected in accordance with the load applied in the full-scale test. If necessary, the load is multiplied by a factor so that it exactly matches the load during the full-scale test. The load selected for the simulation at the compression stage is multiplied by a negative factor. Thus, two peak loading points are determined in the tension-compression cycle.

To assess fatigue, a symmetrical loading cycle is set by indication of the maximum tensile and compressive loads. The loads for numerical fatigue tests were selected in accordance with the value of the load during a full-scale fatigue test. In the computational assessment of fatigue characteristics, the fatigue strength estimation method was used with Goodman correction of average stresses under uniaxial loading.

In Altair HyperLife, any user-defined S-N curve must be specified for a symmetrical loading cycle, and should consist of two linear sections defining the relationship between the durability N_f and the amplitude of stresses during a symmetrical loading cycle:

$$S(N_f) = \begin{cases} S_1 \left(N_f\right)^{-b_1}, & N_f \le N_{limit} \\ FL \left(N_f\right)^{-b_2}, & N_f > N_{limit} \end{cases}, \quad (6)$$

where S is the stress amplitude of the symmetrical cycle (σ_a in Eq. (5)), S_1 is the coefficient of fatigue strength, N_{limit} is the maximum number of cycles before failure, FL is the fatigue limit, b_1 and b_2 are the first and second fatigue strength indicators equal to the slope coefficients of straight lines on a logarithmic scale.

The previously introduced fatigue equation (5) describes the left branch of the S-N curve (Fig. 11), constructed according to Eq. (6), if we take the coefficients $b_1 = B$ and

$S_1 = A$. In addition, for certainty, Fig. 10 shows a view of the fatigue curve with a horizontal right-hand branch corresponding to the exponent $b_2 = 0$, which is a frequently used model case when describing the phenomenon of fatigue in metals.

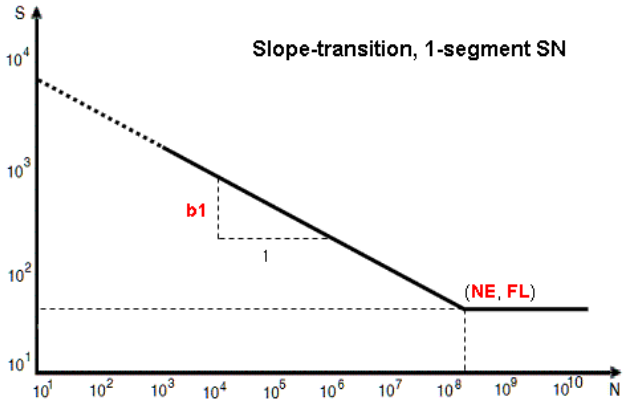

Fig. 10. Scheme of one-segment SN curve

The parameters set for the material model are elastic modulus, Poisson's ratio, ultimate tensile strength of the material, the characteristics of the fatigue curve, namely, the exponent B, the maximum number of cycles to failure N_{limit} and the fatigue limit FL. In our case, elastic modulus was 105 803 MPa, Poisson's ratio was 0.3 and ultimate tensile strength of the material was 906 MPa [22]. The mean computational time to evaluate the fatigue characteristics of one specimen with Altair HyperLife software on an Intel Xeon Silver 4210R processor is 1.8 h.

Results and Discussion

Evaluation of geometric parameters and density

The specimens made of the additively manufactured titanium alloy were subjected to measurements of the geometric dimensions and weighing to assess the quality of 3D printing. The actual dimensions of the specimens are given in Table 2. The mean cross-sectional area in the narrowest point of the gauge section was 17.9 mm^2, and the density of the titanium alloy was 4 305 kg/m^3.

Table 2. Geometric characteristics of solid specimens

Specimen	Gauge thickness *h*, mm	Gauge width *b*, mm	Cross-sectional area *A*, mm^2	Specimen	Gauge thickness *h*, mm	Gauge width *b*, mm	Cross-sectional area *A*, mm^2
1	2.99	5.99	17.91	9	2.98	5.97	17.79
2	3.02	5.99	18.09	10	2.98	5.96	17.76
3	2.98	6.00	17.88	11	2.99	5.99	17.91
4	3.00	6.01	18.03	12	2.99	6.00	17.94
5	2.99	5.98	17.88	13	2.97	5.98	17.76
6	3.00	5.97	17.91	14	2.98	5.98	17.82
7	3.01	6.01	18.09	15	2.97	5.98	17.76
8	2.99	6.00	17.94	–	–	–	–

Specimens of the diamond and gyroid types with three volume fractions of solid material – 30, 50 and 70 % – were printed for the full-scale tests (two identical specimens of each type, 12 specimens in total). The overall dimensions of the gauge cross-section of the metamaterial specimens are given in Table 3. The actual mass of specimen types was determined as the arithmetic mean of the masses of the specimen type entities (Table 4).

Table 3. Geometric characteristics of gauge section of metamaterial specimens

Specimen	Specimen ID	Overall gauge thickness h, mm	Overall gauge width b, mm
1	FD-70-1	14.89	14.61
2	FD-70-2	14.96	14.59
3	FG-70-1	14.90	14.61
4	FG-70-2	14.95	14.61
5	FD-50-1	15.28	14.90
6	FD-50-2	15.29	14.92
7	FG-50-1	15.29	14.91
8	FG-50-2	15.25	14.88
9	FD-30-1	15.03	14.98
10	FD-30-2	15.07	14.97
11	FG-30-1	15.29	14.84
12	FG-30-2	15.21	14.91

Table 4. Actual mass of specimens for fatigue tests

Volume fraction, %	Mass of diamond specimens, g	Mass of gyroid specimens, g
30	54.5	52.4
50	79.9	78.1
70	105.2	104.9

The actual volume fraction of each specimen differs from the nominal value by no more than 5 % (Table 5). The exception is the diamond with the nominal volume fraction of 30 %. Because thinner structural elements were included in this type of meta-biomaterial compared to specimens of other types, the volume fraction of the diamond 30 % specimen was deliberately exceeded by 27.5 % compared to the target at the stage when the model was constructed for printing, since the minimum thickness of the strut was set at 1 mm (radius of 0.5 mm).

Table 5. Actual volume fractions of metamaterial specimens

Volume fraction, %	Volume fraction of diamond specimens, %	Volume fraction of gyroid specimens, %
30	45.7	31.5
50	63.8	51.7
70	72.9	70.8

Results of cyclic tests for specimens made of solid material

The results of the cyclic tests performed with 15 specimens made of additively manufactured Ti-6Al-4V alloy are given in Table 6, including the cyclic load frequency, the load amplitude (also converted to longitudinal stress occurring in the narrowest point of the specimen's gauge section) and fatigue life expressed as the number of loading cycles

that the specimen withstood. The rows are sorted in descending order from the highest load applied to the lowest. One of the prepared specimens (specimen 3) was used only for calibrating the equipment, so its experimental characteristics are not given in Table 6.

Table 6. Parameters of cyclic tests for solid specimens

Load amplitude, F_a, kN	**Stress amplitude, σ_a, MPa**	**Fatigue life, N_f, cycles**	**Test frequency, f,Hz**	**Specimen**	**Note**
13.43	750	2 492	66.7	1	–
9.04	500	9 315	67.5	2	–
7.66	430	31 407	66.8	14	–
7.16	400	49 363	71.3	11	–
5.41	300	180 259	68.0	4	–
4.84	270	195 001	67.9	6	–
4.44	250	769 413	66.8	15	–
4.34	240	403 988	67.5	7	–
4.3	242	–	66.7	13	No failure after 3 877 783 cycles
4.16	232	–	67.9	12	No failure after 4 000 020 cycles
4.13	230	382 689	67.7	8	
4	225	–	68.6	10	No failure after 4 000 008 cycles
3.93	220	–	68.0	5	No failure after 4 000 007 cycles
3.74	210	–	67.5	9	No failure after 4 000 000 cycles
–	–	–	–	3	Reference specimen

The appearance of the specimens after completion of the tests is shown in Fig. 11. As can be seen from the photographs, several specimens (specimens 5, 9, 10, 12, 13) remained intact after reaching the maximum number of loading cycles. The experimental data for the remaining specimens – the values of the stress amplitude of the loading cycle and the number of loading cycles that the specimen could withstand – are plotted in log-log coordinates (Fig. 12). Fatigue failure expectedly occurred in the smallest gauge cross-section, where maximum normal stresses occur along the longitudinal axis of the specimen.

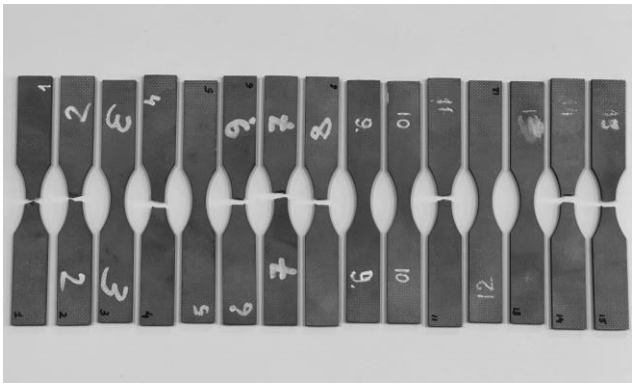

Fig. 11. Solid specimens after fatigue tests

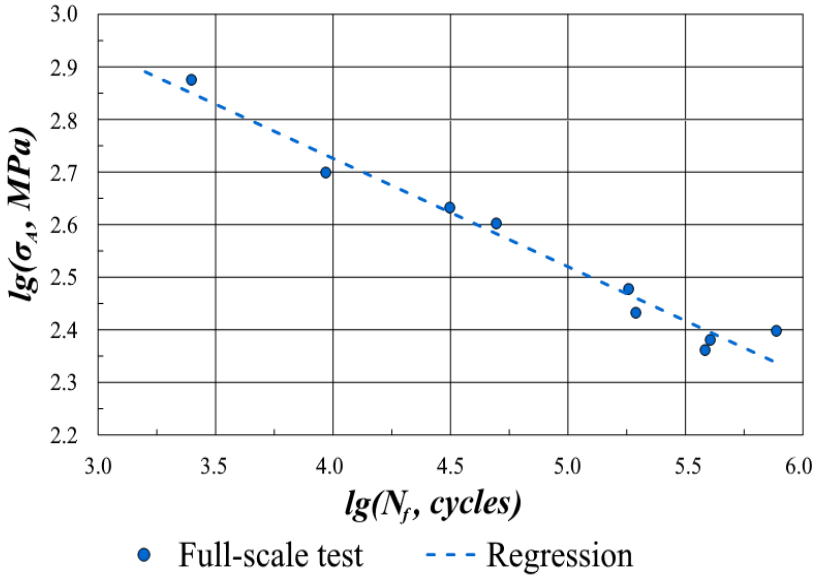

Fig. 12. Experimental results of cyclic tests of solid samples and the regression line in log-log coordinates

A regression dependence was constructed from the experimental points, satisfactorily approximating the linear dependence of the number of loading cycles that the material can withstand on the stresses in the material. The regression coefficients give the values of the exponent B and the amplitude of the fatigue curve of the material (Table 7). The fatigue limit of the Ti-6Al-4V alloy, equal to 213 MPa, was also determined, which is significantly less than the yield strength generally characterizing the strength properties of the material under static loading. Notably, high-cycle failure has a significantly probabilistic nature, and cases when two specimens exhibited significant difference in fatigue life under the same load were observed in full-scale tests.

Table 7. Equation coefficients for inclined branch of fatigue curve for solid material

Fatigue limit after 2 million cycles, FL, MPa	**Equation coefficients for horizontal branch of fatigue curve $\sigma_a(N) = A \cdot N^{-B}$**		
	A, MPa	**B**	**Fatigue life at knee point N_{limit}, cycles**
213	3 547.2	0.206	861 778

Results of cyclic tests of metamaterial specimens

The results of cyclic tests for metamaterial specimens made of additively manufactured Ti-6Al-4V alloy are given in Table 8 and photographs of the specimens after the completion of the tests are shown in Fig. 13. Analysing the results, we found that not all specimens failed under the given cyclic loading: in fact, not only specimens with the high volume fraction of solid material but also specimens with a 30 % volume fraction did not fail.

Table 8 gives the type of specimen, loading cycle frequency, load amplitude (including amplitude converted to longitudinal stress occurring in the narrowest gauge cross-section of the specimen), fatigue life found expressed as the number of loading cycles that the specimen can withstand. The cycle frequency was chosen slightly higher compared to tests of solid materials to shorten the duration of the experiment. Three

specimens did not fail when the maximum number of loading cycles was reached, two of which were specimens with the highest porosity. One specimen failed outside the gauge section, which may be due to a printing defect or stress concentration occurring in the transition zone.

Table 8. Results of full-scale tests for metamaterial specimens

Specimen ID	Load amplitude F_a, N	Fatigue life N_f, cycles	Test frequency, f, Hz	Specimen	Note
FD-70-1	7 000	2 000 000	113.5	1	No failure
FD-70-2	30 000	27 092	129.4	2	–
FD-50-1	8 500	3 818 281	97	5	–
FD-50-2	10 000	1 954 603	96.5	6	–
FD-30-1	5 700	103 175	81.2	9	Failure outside gauge section
FD-30-2	5 100	4 000 083	84.2	10	No failure
FG-70-1	9 500	1 048 331	107.1	3	–
FG-70-2	9 500	638 703	107.2	4	–
FG-50-1	5 100	1 040 982	94.1	7	–
FG-50-2	5 100	799 347	94.2	8	–
FG-30-1	2 100	4 000 000	75.7	11	No failure
FG-30-2	2 500	524 977	75.6	12	–

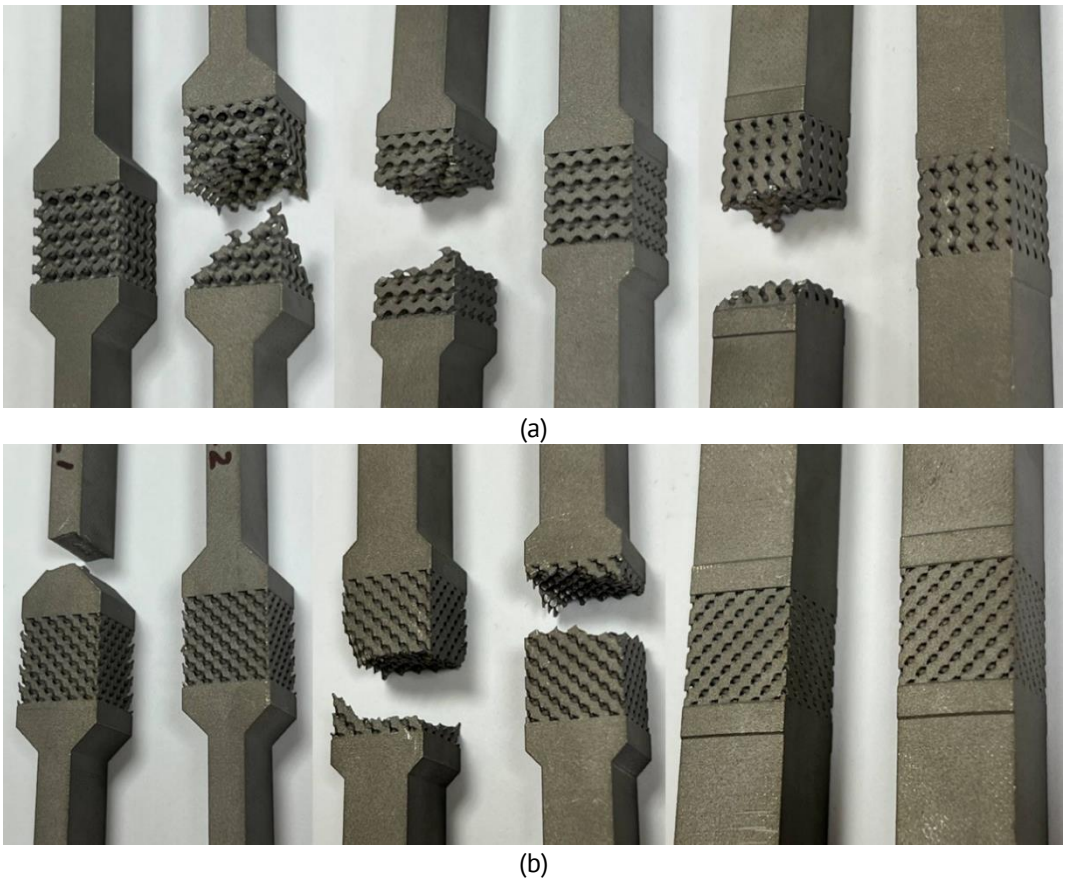

(a)

(b)

Fig. 13. Photographs of specimens after full-scale fatigue tests at time of failure or after reaching the maximum number of loading cycles without failure: (a) from left to right, gyroid specimens, 2 specimens for each volume fraction (30, 50 and 70 %) of solid material, (b) from left to right, diamond specimens, 2 specimens for each volume fraction (30, 50 and 70 %) of solid material

Thus, the presence of a stress concentrator in the grip section of the specimen in the transition from a wider to a thinner part is an essential factor for evaluating the number of cycles to failure in some specimens. Moreover, the selected load turned out to be low for some specimens.

Simulation results for metamaterial specimens

Numerical analysis of the maximum number of loading cycles (i.e., fatigue life in Altair HyperLife terms) was carried out based on static analysis of the stress-strain state of the specimens (Fig. 14).

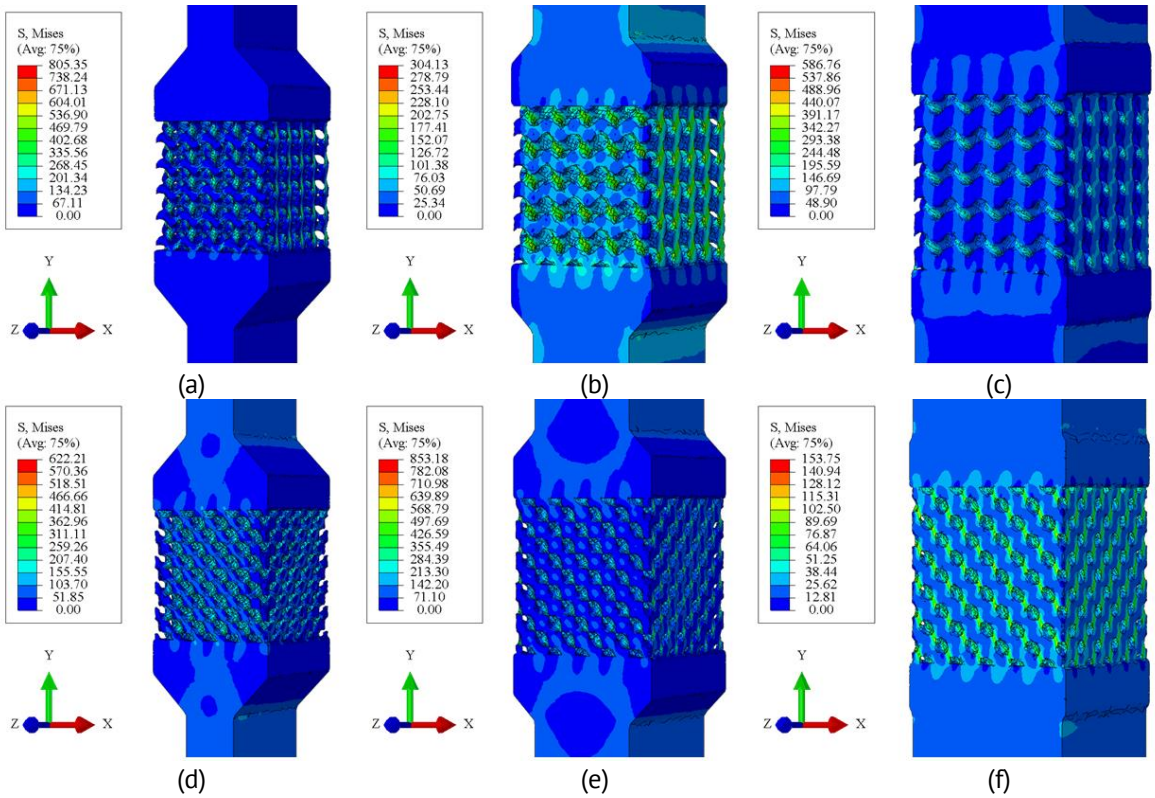

Fig. 14. Distribution of von Mises stress intensity (MPa) for metamaterial specimens with various volume fractions at selected step for analysis in Altair Hyperlife: (a) gyroid 30 %, (b) gyroid 50 %, (c) gyroid 70 %, (d) diamond 30 %, (e) diamond 50 %, (f) diamond 70 %

Figure 15 shows the results as the distribution of the life span, i.e., fatigue life. As can be seen from the fatigue life fields (Fig. 15), all specimens withstood a cyclic load coinciding with the load set during full-scale tests. However, the obtained theoretical values of fatigue life for each specimen turned out to be significantly higher in comparison with the values obtained during full-scale tests. Numerical analysis indicated that the failure did not occur in the specimens.

In view of the above, a parameter C_{finish} responsible for surface roughness of the specimen was introduced into the calculations of the number of cycles to failure (Fig. 16). In this case, the fatigue limit is multiplied by this parameter: $FL' = FL \cdot C_{finish}$.

As already mentioned above, high-cycle fatigue failure is considerably probabilistic in nature, and cases when two specimens had a significant difference in fatigue life at the same load were observed in full-scale tests. Numerical simulation methods do not

allow to detect the precise time of loss of integrity for the specimen, instead providing only the fatigue life for each individual finite element.

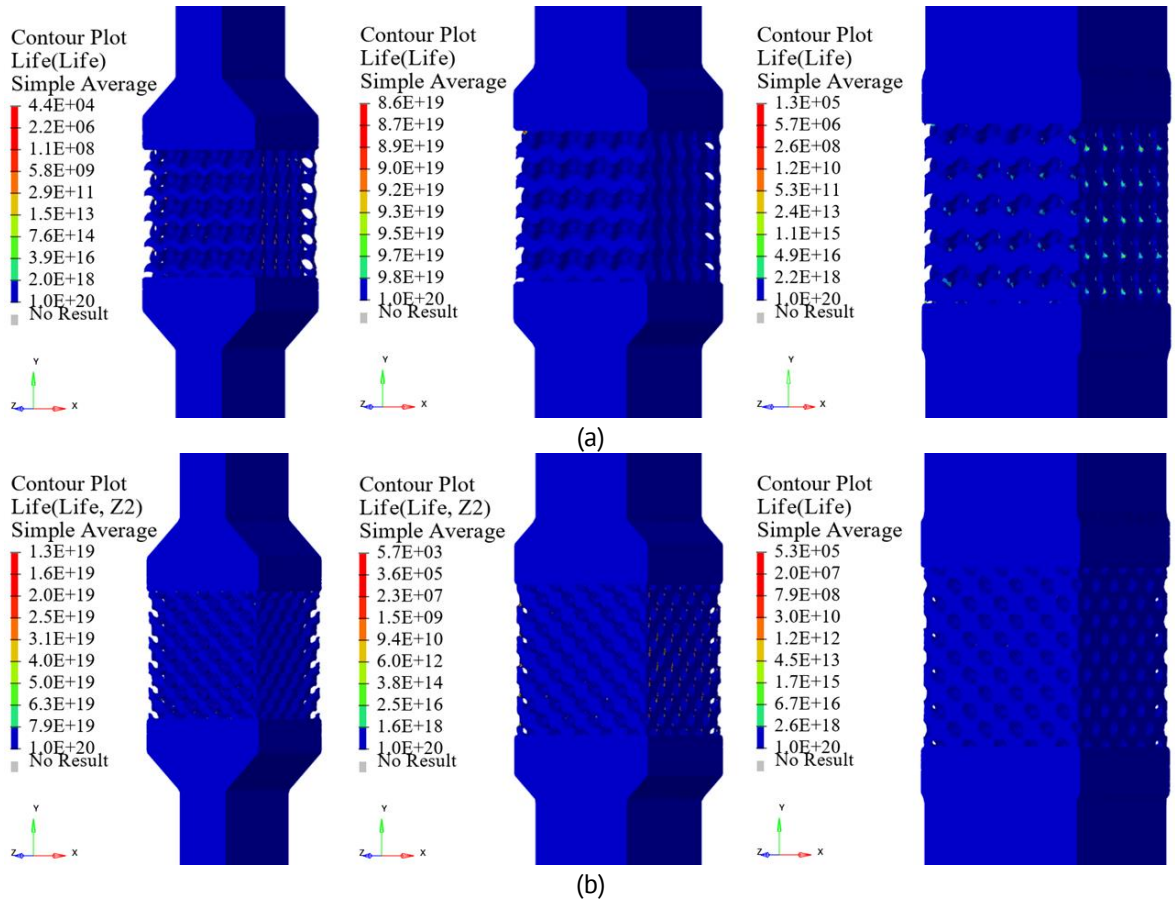

Fig. 15. Numerical estimates for fatigue life based on simulations: (a) from left to right, gyroid specimens with 30, 50 and 70 % volume fractions of solid material, (b) from left to right, diamond specimens with 30, 50 and 70 % volume fractions of solid material

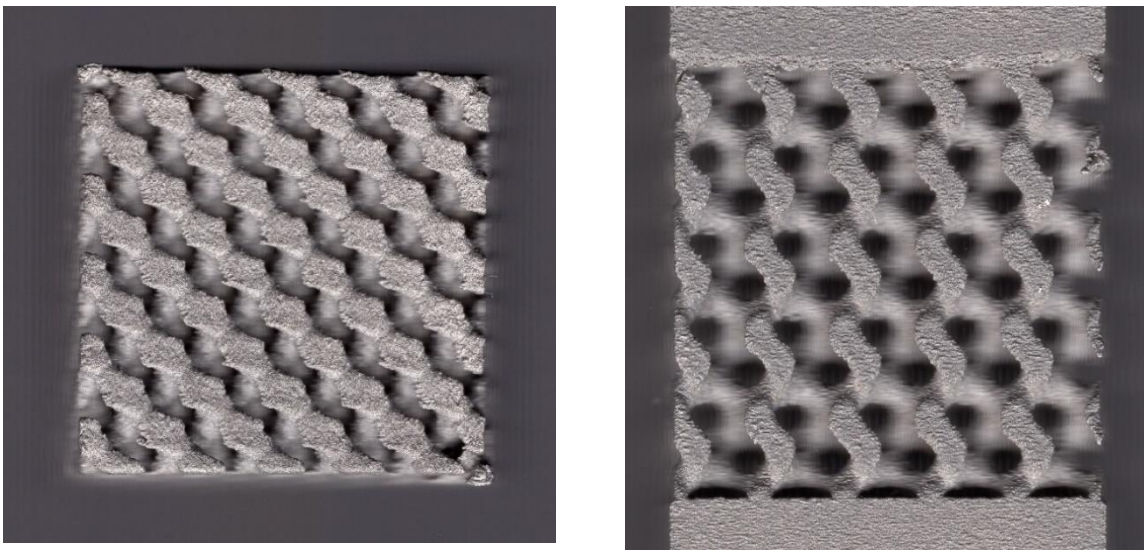

Fig. 16. Photographs for surface of typical specimens, demonstrating poor surface quality of metamaterials obtained by 3D printing

The results of fatigue tests are significantly affected by the surface quality of the specimens and the presence of microcracks and other defects. In the case when meta-biomaterial is produced using additive technologies, this effect becomes key due to the high ratio of surface area to the volume in comparison with conventional solid structures. When cyclic loading with a low amplitude is used to determine the fatigue limit of the material and plot the S-N curve with a large number of cycles (more than 2 million), theoretically extending to a horizontal section, the accuracy of predicting the fatigue life also decreases.

Due to the features of cyclic testing described above, the following approach was used to calibrate the fatigue curve:

1. range of values limited by two obtained results was considered for full-scale tests at a fixed load;
2. adequacy of calibration of the S-N curve was estimated entirely based on the results for all full-scale tests performed;
3. additional parameter C_{finish} was introduced to account for the effect of the surface finish quality;
4. loss of integrity was assumed to occur in the specimen if a significant number of elements (about 50 %) with a fatigue life below the considered value were found in the gauge section at a considered time.

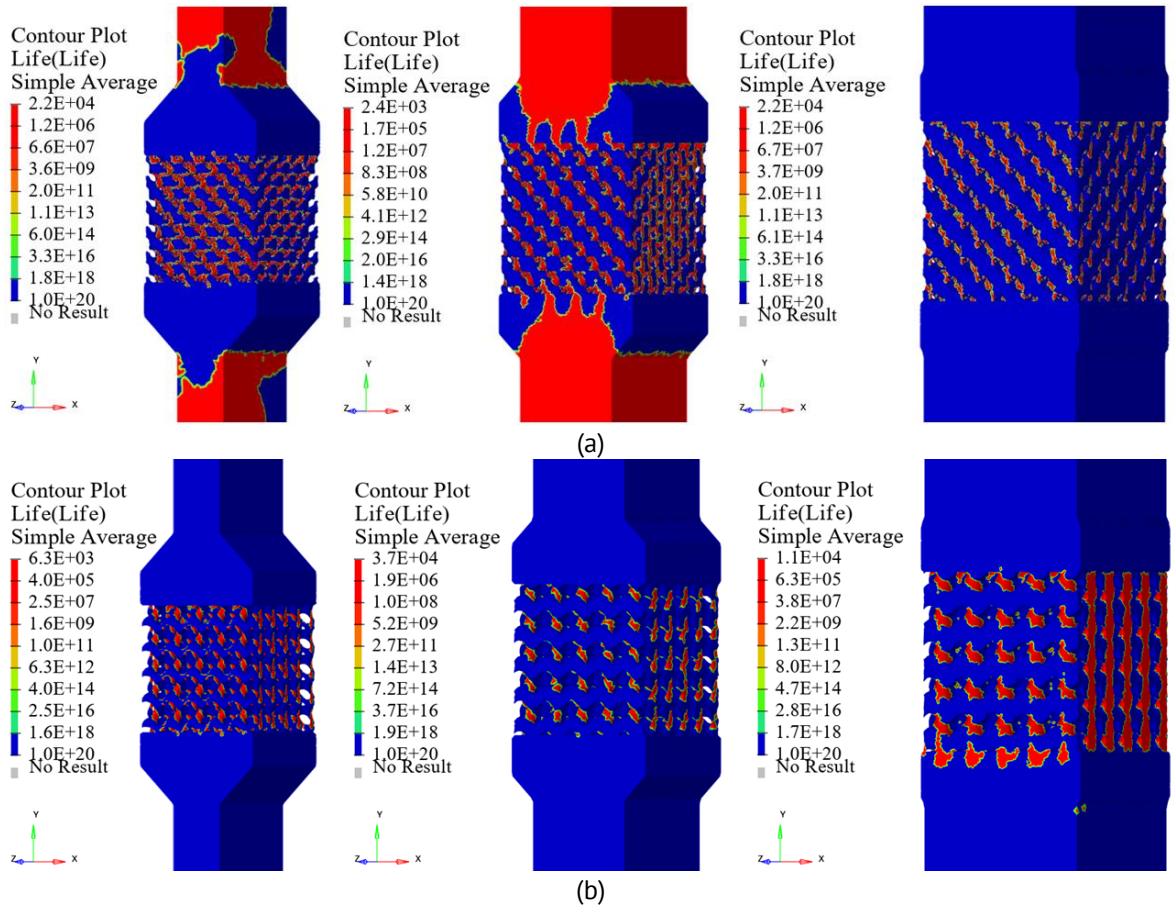

Fig. 17. Numerical estimates for fatigue life based on simulations accounting for the surface roughness parameter: (a) from left to right, gyroid specimens with 30, 50 and 70 % volume fractions of solid material, (b) from left to right, diamond specimens with 30, 50 and 70 % volume fractions of solid material

As a result, we obtained a fitted fatigue model of the material for further calculations with a coefficient of 0.25 accounting for the influence of surface roughness. The simulation results for each full-scale test performed are shown in Fig. 17.

A comparison of the results of full-scale fatigue tests and numerical simulations taking into account the roughness parameter introduced into the numerical model is presented in Table 9. The numerical tests evaluated the volume percentage of the elements in the gauge section of the metamaterial specimen that can withstand the number of cycles obtained during the corresponding full-scale test. This volume did not include the elements in the grips, only the elements in the gauge section. The percentages obtained are listed in the last column of Table 9.

Table 9. Comparison of results of full-scale and numerical (with roughness parameter) fatigue tests

Specimen	Specimen type	Load amplitude F_a, N	Number of cycles to failure for specimen in full-scale tests	Volume percentage of gauge section in FEA model of the specimen withstanding the corresponding number of cycles in full-scale test, %
1	FD-70-1	7 000	2 000 000	63.8
3	FG-70-1	9 500	1 048 331	49.6
4	FG-70-2	9 500	638 703	57.5
6	FD-50-2	10 000	1 954 603	22.6
7	FG-50-1	5 100	1 040 982	67.0
8	FG-50-2	5 100	799 347	67.0
10	FD-30-2	5 100	4 000 083	33.3
12	FG-30-2	2 500	524 977	72.7

Analysing the results of numerical fatigue tests, we observe that the mean percentage of elements in the gauge section that did not fail is 52.4 % for all specimens, with the target value of 50 %. Thus, we estimate the difference between the results of full-scale and numerical fatigue tests as 4.8 %. The degree of agreement between the results allows to conclude that this model of solid material can offer high fidelity in numerical fatigue tests of meta-biomaterial specimens manufactured by additive technologies from Ti-6Al-4V alloy, allowing to expand the range of approaches to numerical analysis of fatigue.

Discussion

Studying the fatigue characteristics of the specimens made of solid titanium and metamaterials, fabricated by selective laser melting, we detected several major trends for further detailed discussion in the context of existing theory.

The obtained values of the fatigue limit for solid Ti-6Al-4V (213 MPa for 2 million cycles) are consistent with the data given in [5,6,23], where values in the range of 200–250 MPa were observed for similar test conditions (symmetrical cycle, $R = -1$). However, there was a significant variance in the results for metamaterials. This can be explained by increased sensitivity of metamaterials to surface defects.

Weighing shows that the actual volume fractions of metamaterials differed from the nominal ones by 5–27 %, which is typical for SLM technologies due to incomplete melting of powder and the presence of pores. It was also noted in [24] that non-optimal

parameter selection of laser melting (for example, insufficient laser power or scan speed) cause porosity and microcracks, reducing the fatigue limit by 15–40 %. Similar conclusions are presented in [25], where the fatigue limit for SLM-printed Ti-6Al-4V turned out to be 25 % lower than that of conventional alloy due to internal defects. Furthermore, the surface roughness that was not taken into account in the initial numerical models considerably influences the simulation results in our case. Introducing a correction factor ($C_{finish} = 0.25$) allowed to reduce the discrepancy between the experimental and computational data to 4.8 %. The effect of the microstructure on the fatigue life of the specimen was also considered in [26].

Using the Goodman approach to mean stress correction in Altair HyperLife yielded good agreement with experimental data after fitting. However, the same as in [27], there were limitations in predicting the fatigue life in the horizontal branch of the S-N curve (after N_{limit}). This is due to probabilistic nature of failure in the region of high-cycle fatigue, where microstructural defects play the dominant role. To improve the simulation accuracy in future studies, it is advisable to include probabilistic methods similar to those proposed in [28].

The Gyroid specimens exhibited more predictable behaviour under cyclic loading compared to Diamond, which is consistent with the results provided in [29] for similar structures. The authors explain this by a uniform stress distribution in Gyroid structures, while stresses in Diamond structures tend to concentrate in the connections between the struts. The study also established that cracking begins to accelerate after reaching maximum strength, resulting in a noticeable deterioration in mechanical properties. For Diamond structures, it is recommended to increase the volume fraction of the elements by 20-30% as reinforcement against fatigue failure [30].

Based on the data obtained and literature analysis, optimization of printing parameters can be proposed to increase the fatigue life of material specimens, for example, preheating the platform to reduce residual stresses as in [31], surface post-treatment, which, according to the data in [32], significantly improves the surface quality of the specimen and, accordingly, slows down cracking in the surface layer. Hybrid models combining machine learning and finite element analysis to account for the stochastic nature of defects can also help improve fatigue life and the prediction quality [33].

Conclusion

The paper reports on the fatigue properties of additively produced metamaterial specimens based on the biocompatible titanium alloy Ti-6Al-4V, using experimental and theoretical approaches using the finite element method. Dynamic full-scale tests were carried out under high-cycle loading below the yield strength of the material.

The fatigue curves obtained experimentally were used to determine the fatigue limits and other characteristics of additively produced solid titanium alloy and the metamaterials based on it. Finite element models of the considered metamaterials were also developed and numerical simulation of the obtained specimens was carried out to evaluate the fatigue life of the specimens taking into account the obtained mechanical properties of the additive titanium alloy. The results of full-scale and numerical tests exhibit qualitatively similar dynamic behaviour. Hypothetically, the discrepancies in

numerical and experimental data are due to the observed printing defects of metamaterials with complex internal structure as well as to poor surface quality of the metamaterials resulting from 3D printing.

While full-scale tests remain the gold standard, their high cost and duration have triggered the search for numerical methods based on computational models. The study confirmed the feasibility of using simulation approaches to predict the fatigue characteristics of titanium metamaterials. Importantly, the surface roughness and possible manufacturing defects should be carefully monitored in additive manufacturing of metamaterials to achieve high accuracy.

Accounting for microstructure and defects is crucial for titanium alloys, while a key aspect for metamaterials is to accurately describe the geometry and damage. In view of this, we can conclude from the results obtained that numerical tests for metamaterials with a low volume fraction (30 %) require additional fitting due to increased sensitivity to defects; in the case of lattice structures, it is important to minimize stress concentrators in the interfaces between the gauge and the grip sections. Further research might focus on integrating machine learning to account for the variability in the properties induced by SLM additive manufacturing.

CRediT authorship contribution statement

Leonid B. Maslov: writing – original draft, writing – review & editing; **Aleksey I. Borovkov**: supervision; **Liliya S. Nezhinskaya**: investigation, conceptualization, writing – original draft; **Mikhail A. Zhmaylo**: data curation, writing – review & editing; **Fedor D. Tarasenko**: investigation.

Conflict of interest

The authors declare that they have no conflict of interest.

References

1. Boyer RR. An overview on the use of titanium in the aerospace industry. *Materials Science and Engineering A-structural Materials Properties Microstructure and Processing.* 1996;213: 103–114.
2. Dudescu MC, Vilau C. Mechanical behaviour of 3D-printed metamaterials with tunable stiffness. *The Romanian Journal of Technical Sciences. Applied Mechanics.* 2019;64(2): 153–161.
3. Lewandowski JJ, Seifi M. Metal Additive Manufacturing: A review of mechanical properties. *Annual Review of Materials Research.* 2016;46(1): 151–186.
4. Bartolomeu F, Gasik M, Silva FS, Miranda G. Mechanical properties of Ti6Al4V fabricated by laser powder bed fusion: a review focused on the processing and microstructural parameters influence on the final properties. *Metals.* 2022;12: 986.
5. Boyer R, Welsch G, Collings EW. *Materials Properties Handbook: Titanium Alloys.* ASM International; 1994.
6. Chernavsky SA, Reshchikov VF. *Metalworker's Handbook. Vol.* 2. Moscow: Mashinostroenie; 1976. (In Russian)
7. Feodosyev VI. *Strength of Materials.* Moscow: Bauman Moscow State Technical University Publishing House, 2018. (In Russian)
8. Akahori T, Niinomi M, Fukui H, Ogawac M, Toda H. Improvement in fatigue characteristics of newly developed beta type titanium alloy for biomedical applications by thermo-mechanical treatments. *Materials Science and Engineering: C.* 2005;3: 248–254.
9. Gunawarman, Niinomi M, Akahori T, Souma T, Ikeda M, Toda H, Terashima K. Fatigue characteristics of low cost β titanium alloys for healthcare and medical applications. *Materials Transactions.* 2005;46(7): 1570–1577.

10. Lütjering G, Williams JC. *Titanium*. Berlin: Springer, 2007.
11. Sterling A, Shamsaei N, Torries D, Thompson SM. Fatigue behaviour of additively manufactured Ti-6Al-4V. *Procedia Engineering*. 2015;133: 576–589.
12. Arcari A, Apetre NA, Strickland EP, Michopoulos J. On the assessment of low cycle fatigue performance of octet-based structural metamaterial. *International Journal of Fatigue*. 2025;197(8): 108936.
13. Li PY, Sun WB, Zhang W, Ma YE. Effect of geometric defects on the mechanical properties of additive manufactured Ti6Al4V lattice structures. *Thin-Walled Structures*. 2024;205(15): 112497.
14. Rodrigues JP, Thanumoorthy RS, Manjhi SK, Sekar P, Perumal DA, Bontha S, Balan ASS. Hybrid additive manufacturing of ER70S6 steel and Inconel 625: A study on microstructure and mechanical properties. *Materials Today Communications*. 2023;37: 106977.
15. Liu L, Kamm PH, García-Moreno F, Banhart J, Pasini D. Elastic and failure response of imperfect three-dimensional metallic lattices: the role of geometric defects induced by selective laser melting. *Journal of the Mechanics and Physics of Solids*. 2017;107: 160–184.
16. Yaghoobi M, Chen Z, Sundararaghavan V, Daly S, Allison JE. Crystal plasticity finite element modeling of extension twinning in we43 mg alloys: calibration and validation. *Integrating Materials and Manufacturing Innovation*. 2021;10: 488–507.
17. Bao H, Wu S, Wu Z, Kang G, Peng X, Withers PJ. A machine-learning fatigue life prediction approach of additively manufactured metals. *Engineering Fracture Mechanics*. 2021;242: 107508.
18. Interstate Standard. GOST 25.502-79. *Strength analysis and testing in machine building. Methods of metals mechanical testing. Methods of fatigue testing*. Moscow: Standardinform; 2005. (In Russian)
19. Borovkov AI, Maslov LB, Zhmaylo MA, Tarasenko FD, Nezhinskaya LS. Elastic properties of additively produced metamaterials based on lattice structures. *Materials Physics and Mechanics*. 2023;51(7): 42–62.
20. Borovkov AI, Maslov LB, Zhmaylo MA, Tarasenko FD, Nezhinskaya LS. Finite element analysis of elastic properties of metamaterials based on triply periodic minimal surfaces. *Materials Physics and Mechanics*. 2024;52(2): 11–29.
21. Troshchenko VT, Sosnovsky LA. *Fatigue Resistance of Metals and Alloys*. Kyiv: Naukova Dumka; 1987. (In Russian)
22. Nezhinskaya LS, Borovkov AI, Maslov LB, Zhmailo MA, Tarasenko FD. Study of elastic-plastic properties of meta-biomaterials. Natural and virtual tests. In: *Proc. XXIV Winter School on Continuum Mechanics Perm, February 24–28, 2025*. Perm: PFRC UB RAS; 2025. p.198–199. (In Russian)
23. Leyens C, Peters M. *Titanium and Titanium Alloys: Fundamentals and Applications*. Weinheim: Wiley-VCH, 2003.
24. DebRoy T, Wei HL, Zuback JS, Mukherjee T, Elmer JW, Milewski JO, Beesea AM, Wilson-Heida A, De A, Zhang W. Additive manufacturing of metallic components – Process, structure and properties. *Progress in Materials Science*. 2018;92(3): 112–224.
25. Leuders S, Thöne M, Riemer A, Niendorf T, Tröster T, Richard HA, Maier HJ. On the mechanical behaviour of titanium alloy TiAl6V4 manufactured by selective laser melting: Fatigue resistance and crack growth performance. *International Journal of Fatigue*. 2013;48: 300–307.
26. Wang H, Zhou K, Tian Z, Xie D, Yang Y, He Y, Wang L, Lv F, Shen L. Fatigue performance at ultra-low porosity of Ti6Al4V produced by laser powder bed fusion after post heat treatment. *SSRN* [Preprint] 2022. Available from: dx.doi.org/10.2139/ssrn.4224194.
27. Przybyla C, McDowell D. Microstructure-sensitive extreme-value probabilities of high-cycle fatigue for Ni-base superalloy IN100. *International Journal of Plasticity*. 2010;26(3): 372–394.
28. Fatemi A, Socie D. A critical plane approach to multiaxial fatigue damage. *International Journal of Fatigue*. 1988;10(2): 149–165.
29. Al-Ketan O, Adel Assad M, Abu Al-Rub RK. Mechanical properties of periodic interpenetrating phase composites with novel architected microstructures. *Composite Structures*. 2017(3);176: 9–19.
30. Xu S, Shen J, Zhou S, Huang X, Xie YM. Design of lattice structures with controlled anisotropy. *Materials & Design*. 2016(3);93: 443–447.
31. Vrancken B, Thijs L, Kruth JP, Humbeeck JV. Heat treatment of Ti6Al4V produced by Selective Laser Melting: Microstructure and mechanical properties. *Journal of Alloys and Compounds*. 2012;541: 177–185.
32. Sokolnikov VN, Sukhochev GA, Usov SV, Tochilin IP. Study of the surface layer of a part after a combined mechanical-electrochemical hardening process. *Hardening Coating Technologies*. 2019;15(12): 555–560. (In Russian)
33. Zhan Z, Hu W, Meng Q. Data-driven fatigue life prediction in additive manufactured titanium alloy: A damage mechanics based machine learning framework. *Engineering Fracture Mechanics*. 2021;252(7785): 107850.